DGLR
Satzspiegelfeld

Experimental Investigation of Tip Clearance Noise in Axial Flow Machines

Dipl.-Ing. F. Kameier*, Dipl.-Ing. T. Nawrot* and Dr.-Ing. W. Neise**
*Hermann-Föttinger-Institut TU Berlin
**Deutsche Forschungsanstalt für Luft- und Raumfahrt (DLR)
Abteilung Turbulenzforschung
Müller-Breslau-Str. 8, D-1000 Berlin 12

ABSTRACT

An experimental investigation is described to identify the aeroacoustic generation mechanism of the tip clearance noise of axial turbomachines. The tip clearance flow is a secondary flow through the radial gap between the blade tip and the casing wall which is driven by the pressure difference between suction side and pressure side of each blade. Tip clearance noise can be a significant source of noise when the tip clearance exceeds a certain limit.

It is well known that a small tip clearance is beneficial for both the aerodynamic performance and the noise characteristics of axial flow machines.

In this paper experimental results of an ongoing study into the nature of the tip clearance noise are presented. Also, some experimental obversations regarding a hysteresis-type behavior of the aerodynamic fan performance and rotating stall inception are reported.

1. INTRODUCTION

A number of aerodynamic investigations have been concerned with flow relationships in the blade tip area of the fan and in the radial gap of axial flow machines. From these, it is well known that large gap widths cause large regions of reversed flow which in turn lead to pressure losses and increased sound power levels. The aeroacoustic noise generation mechanism, however, which is set up by an enlarged tip clearance gap remains widely unknown.

LONGHOUSE [1], MARCINOWSKI [2], STÜTZ [3] and FUKANO et al.[4] characterize tip clearance noise as broad banded. On the other hand, an earlier investigation of the present research group [5] on a simple industrial fan (D=0.314 mm, hub-tip ratio 0.57) has shown that increasing the tip clearance results in drastic level increases, i.e., up to 10 dB, in the radiated sound pressure spectrum within limited, almost narrow-band frequency regions.

Besides studying the general aeroacoustic characteristics of axial fans associated with tip clearance noise, an attempt has been made here to localize the source regions of the various noise components by using flush mounted microphones in the casing wall, miniature pressure sensors (KULITE) on the impeller blades, and a pitot-type unsteady pressure probe in the blade tip flow regime.

Variations of the aerodynamic operating conditions gives insight into the generation of different noise components appearing at varying frequencies and into the formation characteristic of rotating stall.

2. EXPERIMENTAL FACILITY

A schematic view of the experimental setup is shown in Figure 1 along with its major dimensions. For most of the tests, only a bellmouth nozzle was mounted on the fan inlet side. The anechoically terminated outled duct is in

NOMENCLATURE

A	= cross-sectional area of the test ducts (A_0=1 m²)
A_c	= cross-sectional area of the fan casing
BPF	= blade passing frequency
CN	= clearance noise
CNF	= clearance noise frequency
c_{ax}	= mean flow velocity
D	= rotor diameter
f	= frequency
Δf_b	= filter bandwidth
L_p	= pressure level re 20 µPa
L_w	= sound power level re 1pW
L_{w_s}	= specific sound power level = $L_w - 10\lg(\dot{V}/\dot{V}_0) - 20\lg(\Delta p_t/\Delta p_{to})$
n	= rotor speed
p	= pressure
Δp_t	= total pressure rise (Δp_{to}=1 Pa)
$\tilde{p}$	= rms-value of pressure fluctuations
Re	= Reynolds-number = $\frac{UD}{\nu}$
RF	= rotor shaft frequency
RS	= rotating stall
RSF	= rotating stall frequency
t	= time
TN	= turbulence noise
TNF	= turbulence noise frequency
St	= Strouhal-number = $\frac{f\,D}{U}\frac{\pi}{Z}$
U	= rotor tip speed
V	= number of stator vanes
$\dot{V}$	= flow rate ($\dot{V}_0$=1 m³/s)
x	= radial distance from casing wall
z	= axial distance from blade leading edge
Z	= number of rotor blades
φ	= flow coeffizient = $\frac{\dot{V}}{U\,A_c}$
$\varphi_{opt.}$	= flow coeffizient at $\eta_{max.}$-point
Φ	= phase angle
γ^2	= correlation coeffizient
ψ	= pressure coeffizient = $2\,\Delta p_t/(\rho U^2)$
η	= efficiency = $\dot{V}\Delta p_t/(W\,\eta_{el})$
η_{el}	= efficiency of the DC-motor
ν	= kinematic viscosity of air
ρ	= density of air
τ	= dimensionless tip clearance normalized with D
ξ	= dimensionless distance from casing wall = x/D
ζ	= dimensionless distance from blade leading edge=z/D

accordance with the standardized in-duct method (ISO 5136, DIN 45 635 Teil 9 [6,7]). A 1/2-inch microphone equipped with a turbulence screen is mounted in a rotatable duct section to measure the circumferentially averaged sound pressure level. Some measurements were made with an anechoic test duct on the inlet side. The design of the inlet duct is principally the same as that of the outlet duct.

The fan rotor is 452.4 mm in diameter with a hub-to-tip ratio of 0.62. There are 24 blades with a profile similar to the NACA 65 series. The cord length is 43 mm at the tip, and the maximum blade thickness is 3 mm. The blade stagger angle amounts to 27 degrees at the outer circumference. The stator row comprises 17 non-profiled vanes. The fan design is similar to a high pressure axial flow machine produced by VOITH-NOVENCO GmbH, Heidenheim, Germany. VOITH-NOVENCO kindly supplied the blades of the impeller.

The impeller diameter is kept constant throughout all experiments described here, while the tip clearance is varied by changing the casing diameter. Four different casing segments were used to give gap widths of 0.3, 0.6, 1.2, and 2.4 mm. Each segment is cylindrical over a length of one impeller diameter upstream of the rotor. Fan impeller and casings segments were machined to be circular and concentric to within 0.01 mm. The four casing segments are connected to the inlet nozzle and the stator section of the fan casing via various conical transition sections. To eliminate problems with flow separation, all transition sections involve an area contraction, so that a negative pressure gradient is ensured.

The fan performance is determined by measuring the static pressures in the inlet nozzle and outlet duct; MKS pressure transducers were used to convert pressures into electrical voltages. The fan efficiency is estimated by measuring the electrical input power of the drive motor, taking its efficiency η_{el} into account. Furthermore, the air-temperature, motor-voltage and -current were measured by using a data acquisition unit, HP 3421A. A computer, HP 9826S, controlled the HP data unit, microphone amplifiers B&K 2636, a two-channel dynamic signal analyzer, HP 3562A, and the rotating ducts for the sound pressure level measurements according to ISO 5136 [6].

The pressure fluctuations on the interior casing wall are measured by 1/8-inch Microphones, B&K 4138, mounted flush with the inner wall. Miniature sensors KULITE LQ 47-5 SG are mounted on the rotating blades to measure the unsteady blade pressures. The low-voltage output signals of the sensors are amplified and then transmitted into the fixed frame of reference by using a two-channel DATATEL telemetry-system.

3. EXPERIMENTAL RESULTS

3.1 AERODYNAMIC AND ACOUSTIC FAN PERFORMANCE

Figure 2a shows the aerodynamic and acoustic fan performance for four tip clearances at a constant speed of 1400 rpm. The range of operating conditions which is of most interest here is circled in Figure 2a and shown in an expanded scale in Figures 2 c-d. Decreasing the tip clearance ratio from τ=0.0053 to τ=0.0027 causes a hysteris region to appear at flow rates somewhat lower than that of optimum operation (η_{max}-point). The hysteresis type behavior becomes more pronounced, when the tip clearance ratio is further reduced to τ=0.0013 and τ=0.00067. The fan performance in this region is characterized by sudden drops in flow rate, fan pressure, and efficiency and by accompanying increases in specific sound

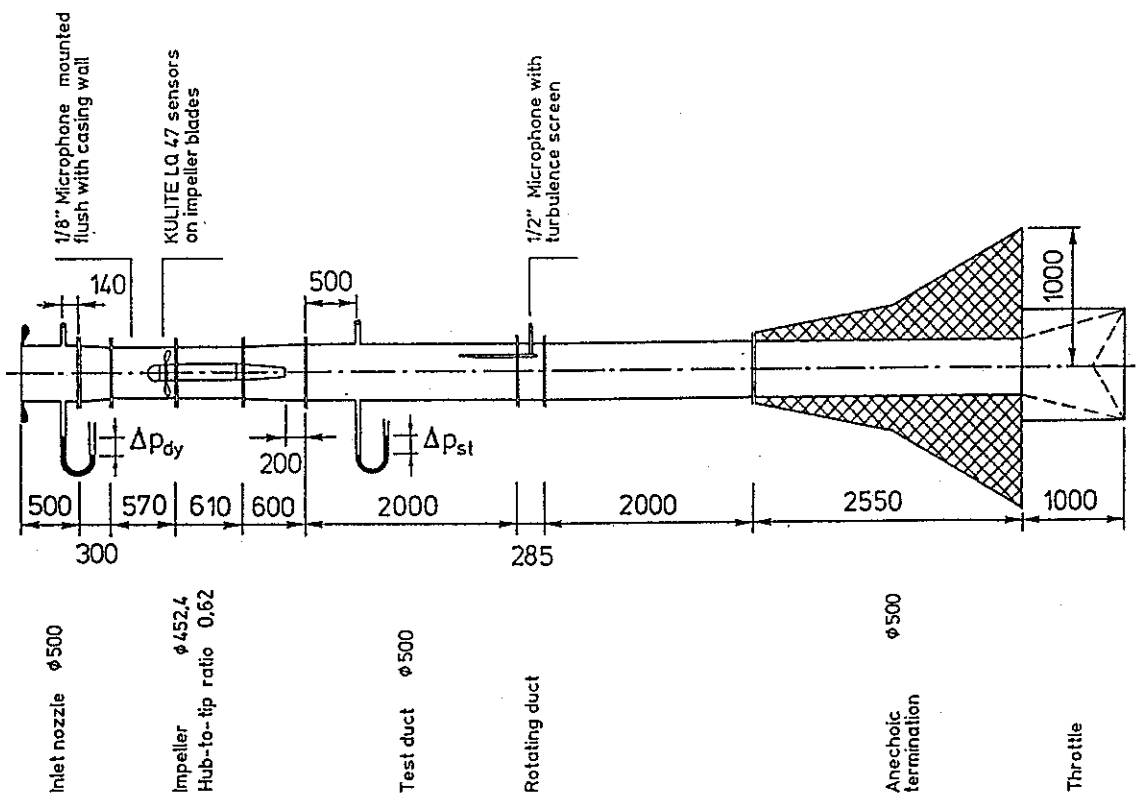

FIG. 1. Experimental set-up (Dimensions in mm.).

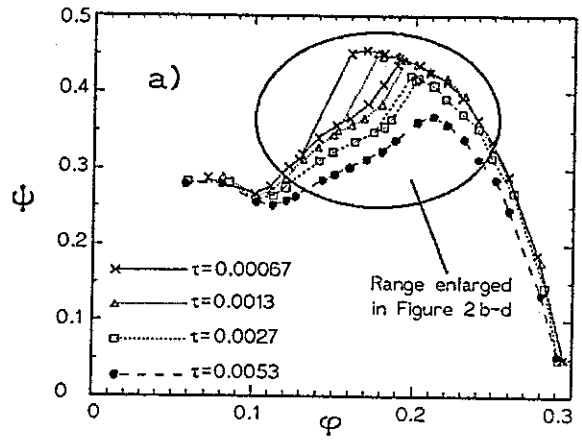

FIG. 2a-d. Effect of tip clearance on the aerodynamic and acoustic stage performance, n=1400 rpm.

power level when the flow is throttled beyond a certain limit. Note that the change in specific sound power level is as much as 20 dB at small tip clearance ratios. When the flow is unthrottled again, the fan performance changes gradually until the original performance characteristic is regained. Only at the largest tip clearance ratio (τ=0.0053) no hysteresis type behavior is found, however, there still is a sudden change in performance, in particular in the specific noise level when the flow rate throttled beyond φ=0.212.

Figure 2d shows that decreasing the tip clearance ratio from τ=0.0053 to 0.00067 increases the optimum efficiency by as much as 7 percent points; the largest improvement occurs when the tip clearance ratio is reduced from τ=0.0053 to 0.0027, i.e., 5 percent points. Incidentally, the efficiency data shown are somewhat lower than commonly found in these types of flow machines, but this is due to the fact that the stator vanes were designed for a much higher impeller speed (n=3000 rpm).

For clarity, the range of flow rates to the right of the hysteresis regime is termed here "stable operating condition" and the rest "unstable operating conditions".

It is obvious from Figure 2 that the onset of unstable fan operation depends on the tip clearance ratio. In Figure 3, the total fan pressure generated at the last stable operating point, i.e., to the very right of the unstable regime, divided by the

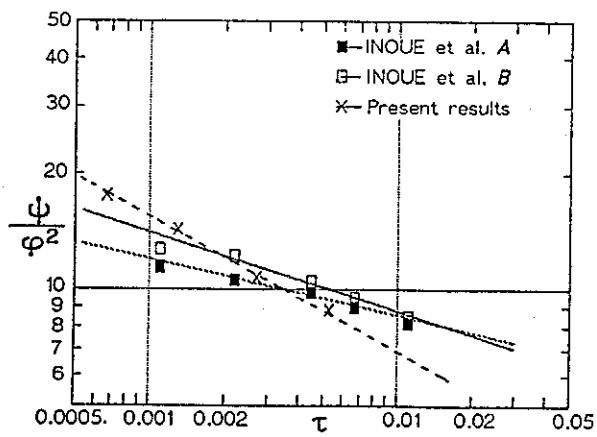

FIG. 3. Pressure/velocity squared - relationship at the last stable fan operating condition.

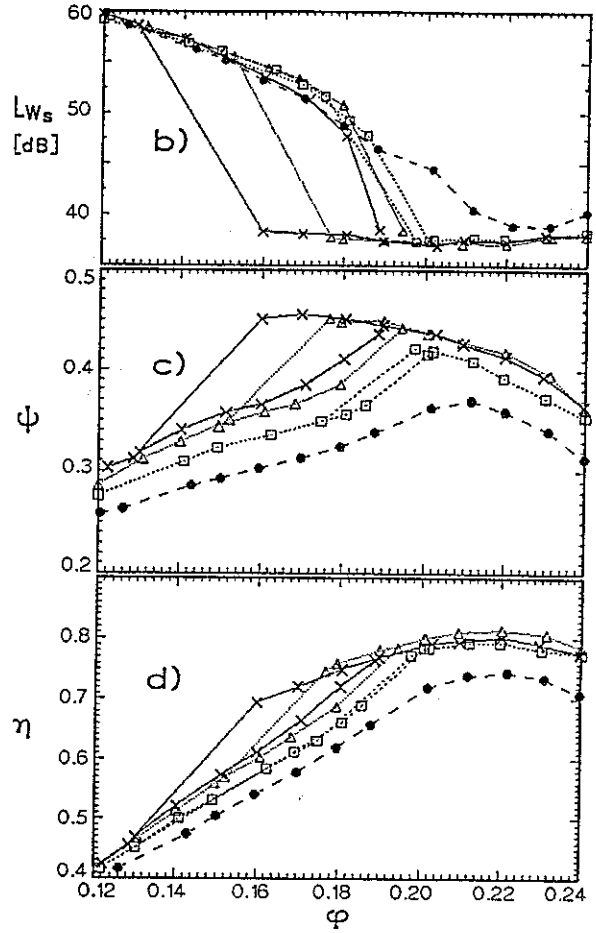

square of the axial flow velocity in the fan duct is plotted as a function of tip clearance ratio, making use of the following proportionality

$$\frac{\Delta p_t}{\rho c_{ax}^2} \sim \frac{\psi}{\varphi^2} \quad . \qquad (1)$$

The experimental data can be approximated by

$$\frac{\psi}{\varphi^2} = \tau^x + K \quad , \qquad (2)$$

where the exponent x and the constant K seem to depend on the blade geometry (profile, stagger angle, blade twist) as is obvious from the comparison with experimental data from INOUE et al. [8] which were measured on two axial compressor stages. The conclusion to be drawn from the above consideration is that a certain pressure difference between suction side and pressure side of the blades is necessary to drive a strong enough secondary blade tip flow against the main flow to enforce unstable flow conditions over entire blade span; this pressure difference is a function of the tip clearance.

3.2 PRESSURE SPECTRA

In the published literature [1], [2], [3] and [4], increases in broadband noise are reported as the result of an enlarged tip clearance. The sound pressure spectra depicted in Figure 4 support this finding.

Figure 5 shows only the low frequency range of the spectra with an enhanced frequency resolution; there it is obvious that enlarging the tip clearance results in drastic level increases in the radiated sound pressure spectra within limited, almost

narrow-band frequency regions. A particulary steep level increase of 15 dB occurs at 370 Hz when the tip clearance ratio is raised from τ=0.0027 to τ=0.0053.

At some frequencies the increase in sound level due to the enlarged tip clearance is masked by acoustic resonance effects related to higher-order duct modes. The cut-off frequency of the first cross mode in the test duct of 500 mm diameter is 399 Hz, and in the fan annulus higher-order modes become propagational beginning at 296 Hz. The spike at 300 Hz is attributed to noise radiation from the thyristor-controlled DC-motor, which is intensified by the acoustic resonances in the fan annulus.

Figures 4 and 5 show the influence of the tip clearance ratio on the radiated sound pressure spectrum for a constant aerodynamic loading condition ($\varphi=\varphi_{opt.}$=0.22). When the flow is

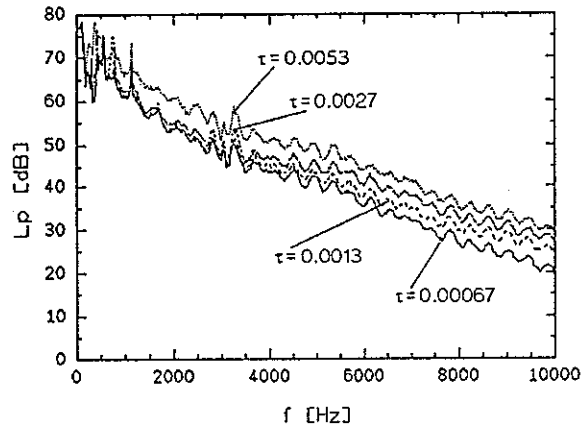

FIG. 4. Sound pressure spectra in the outlet duct as a function of tip clearance τ, $\varphi/\varphi_{opt.}$= 1, n=1400 rpm, Δf_b=12.5 Hz.

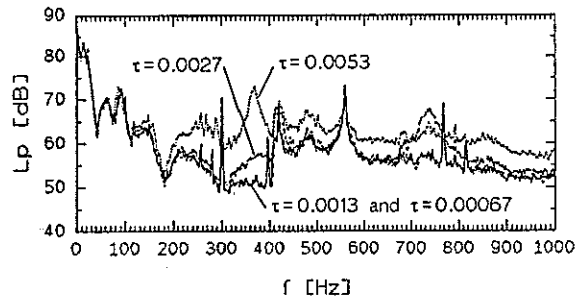

FIG. 5. Sound pressure spectra in the outlet duct as a function of tip clearance τ, $\varphi/\varphi_{opt.}$= 1, n=1400 rpm, Δf_b=1.56 Hz.

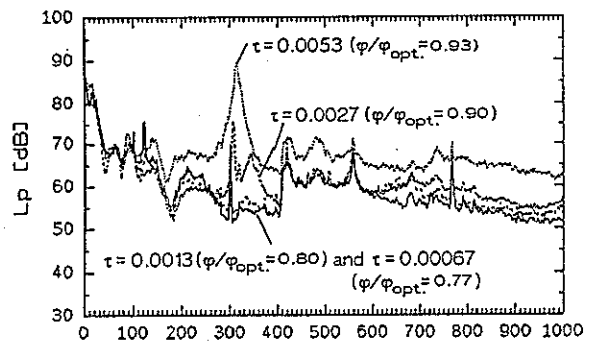

FIG. 6. Comparison sound pressure spectra in the outlet duct at operating conditions with maximum tip clearance noise, n=1400 rpm, Δf_b=1.56 Hz.

throttled, the level of the noise components associated with the tip clearance flow is increased. In Figure 6 are depicted the sound pressure spectra measured at the fan operating conditions at which the tip clearance related noise levels are highest. At the two smallest tip clearance ratios (τ=0.00067 and τ=0.0013) no significant effect of tip clearance is found; here throttling the flow only produces rotating stall at flow rates of $\varphi/\varphi_{opt.}$=0.77 and $\varphi/\varphi_{opt.}$=0.80, respectively.

3.3. INFLUENCE OF INLET FLOW CONDITIONS ON TIP CLEARANCE NOISE

The effect of enlarging the tip clearance on the radiated fan noise seems to be largely independent of the flow conditions at the fan inlet. In Figure 7 the sound pressure spectra in the outlet duct are compared for the cases with and without a test duct on the inlet side (τ=0.0053). In the first case the velocity profile entering the impeller blade row is that of a turbulent duct flow, and in the second case it is uniform. There is hardly any change in the tip clearance noise component. The changes in sound pressure level below 200 Hz are due to axial resonances in the short duct section between inlet nozzle and fan when there is no anechoic termination.

Figure 8 shows a comparison of the sound pressure spectra measured in the inlet duct and the outlet duct. The tip clearance noise is found nearly the same in both ducts.

From Figures 7 and 8 one concludes that monitoring the noise on one side of the fan only is sufficient to study the generation of tip clearance noise. Therefore, only the set-up with no inlet test duct was used for further experiments.

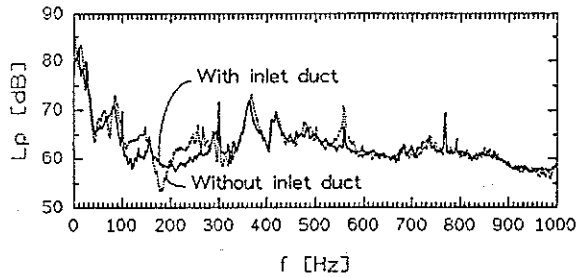

FIG. 7. Sound pressure spectra in the outlet duct measured with and without the test duct on the inlet side, τ=0.0053, $\varphi/\varphi_{opt.}$= 1, n=1400 rpm, Δf_b=1.56 Hz.

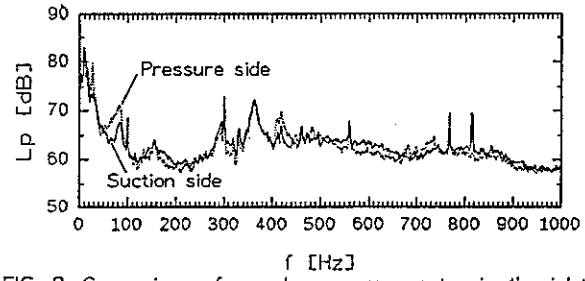

FIG. 8. Comparison of sound pressure spectra in the inlet duct and the outlet duct, τ= 0.0053, $\varphi/\varphi_{opt.}$= 1, n=1400 rpm, Δf_b=1.56 Hz.

3.4. PRESSURE FLUCTUATIONS IN THE ACOUSTIC NEAR FIELD AND FAR FIELD

In Figure 9 pressure spectra are compared which were measured in the outlet duct and at the casing wall at an axial

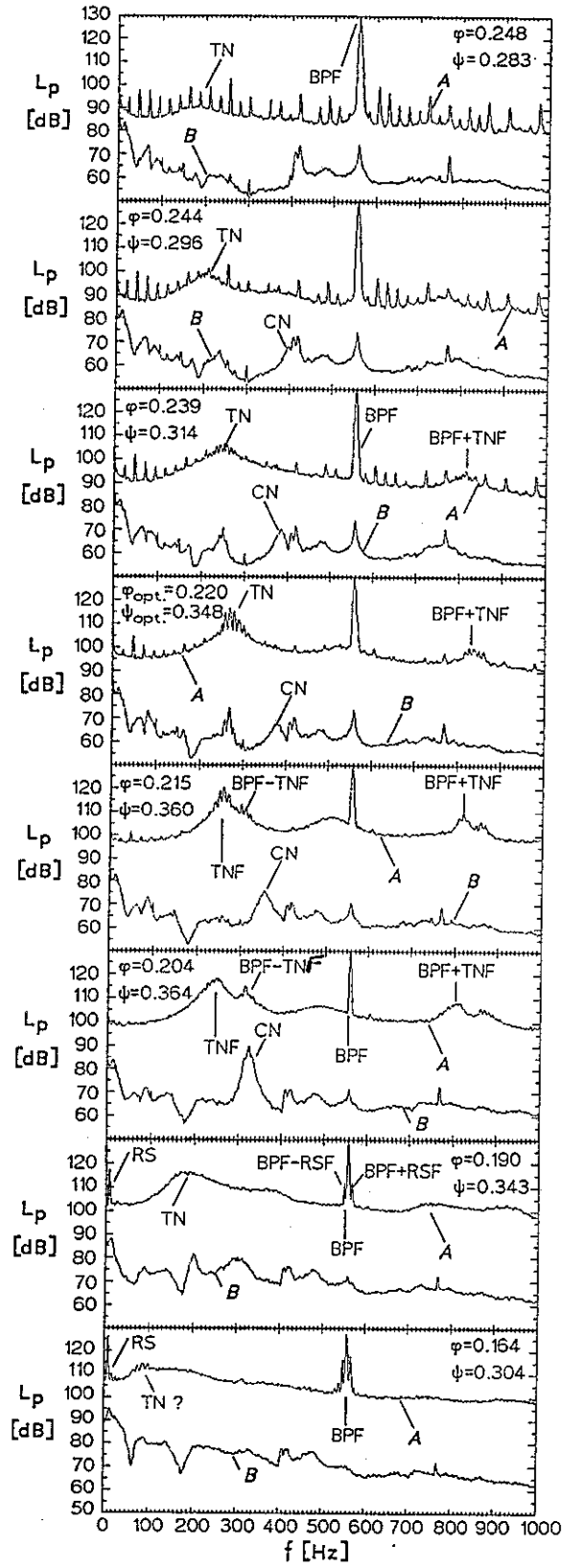

FIG. 9. Pressure spectra in the outlet duct (*B*, far field) and at the casing wall (*A*, ζ=-0.007, near field) for various operating conditions, τ=0.0053, n=1400 rpm, Δf_b= 1.56 Hz.

location ζ=z/D=-0.007 upstream of the leading edge of the impeller blades. These experiments were made with the largest tip clearance ratio τ=0.0053 where the tip clearance noise is most prominent in the spectrum. The outlet duct spectra were obtained as before by using a 1/2-inch slit-tube microphone, and 1/8-inch microphones mounted flush with the inner duct wall were used to measure the near-field pressures. The flow coefficient φ is reduced from the top to the bottom diagram; the corresponding data for the pressure coefficient are also given. The blade passing frequency component (BPF) is clearly visible in the wall pressure spectra, and multiples of the rotor frequency (RF) appear to both sides of this component. The tip clearance noise component (CN) measured in the duct is shifted towards lower frequencies as the flow rate is reduced. In the wall pressure spectra another component termed turbulence noise (TN) appears, which increases in level as the flow rate is throttled. At some operating conditions, tone components exist at frequencies equal to the sum or difference of the blade passing frequency and turbulent noise frequency, i.e., at BPF+TNF and BPF-TNF.

At φ=0.204 (3rd diagram from the bottom) the tip clearance noise reaches its highest level with an increase of 13 dB compared to the flow rate φ=0.215. The frequency of this component is here equal to the difference between blade passing frequency and turbulence noise frequency (CNF=BPF-TNF); this indicates that there is some kind of a resonance effect which is responsible for the drastic increase in tip clearance noise. The physical mechanism for this, however, is not yet understood.

At flow rates below φ=0.204, fan operation becomes unstable, and a tonal component is generated in the wall pressure spectrum below the rotor shaft frequency which is related to rotating stall (RS). This also results in a frequency modulation of the blade passing frequency, and consequently side bands at BPF+RSF and BPF-RSF appear in the wall pressure spectrum.

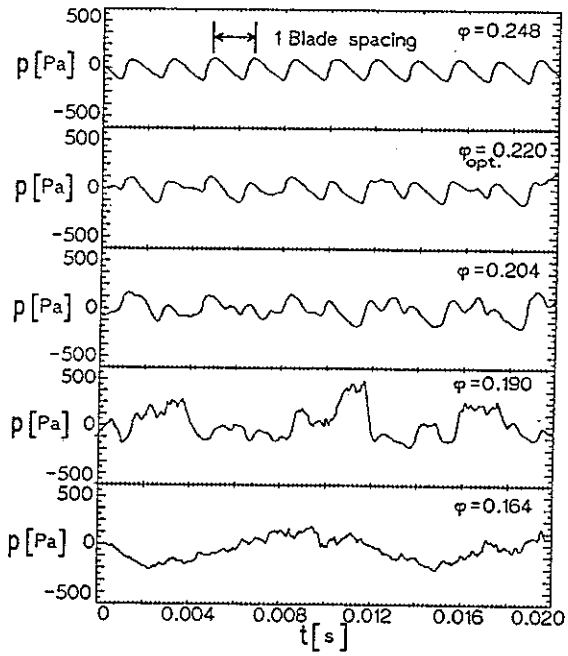

FIG. 10. Time history of wall pressure fluctuations for various operating conditions, τ=0.0053, ζ=-0.007, n=1400 rpm.

Experimental results similar to Figure 9 were also obtained for the other tip clearance ratios which are not shown here. One important observation, however, is that at the two smallest tip clearance ratios, τ=0.00067 and τ=0.0013, not only is the clearance noise component missing in the far field sound spectra (compare also Figure 6) but also the turbulence noise component in the wall pressure spectra. This clearly indicates the importance of the latter component for the tip clearance noise effect.

In Figure 10 instantaneous traces of the time history of the wall pressure fluctuations are shown which correspond directly to the wall pressure spectra described in Figure 9, however, for a smaller number of operating conditions only. With negligible turbulence noise components in the spectrum (φ=0.248), the wall pressure time history is characterized by a strictly regular pattern which is caused by the impeller blades passing by the microphone. When the flow is throttled, deformations of this pattern are observed, and a broad hump appears in the spectrum (turbulence noise). Discrete frequency lines are superimposed on this hump which are also visible in the far-field spectrum (φ=0.22). If the volume flow is reduced further, into the unstable fan operation regime (φ=0.190), the wall pressure time history exihibits distorted patterns moving relative to the blades which indicates the presence of rotating stall.

The onset of the first deformation of the regular wall pressure pattern depends on tip clearance: the smaller the radial gap between blade tip and casing wall, the further the flow can be throttled before the turbulence noise component is generated.

In Figure 11 instantaneous time histories of the wall pressure are shown for two different tip clearance ratios. Note that the total time span covered is ten times larger than in Figure 10. For both tip clearance ratios the fan is operated in the rotating stall region. This is particularly evident in the lower diagramm (τ=0.0027) where a regular pattern is found over part of the circumference while the rest of the pressure signature is distorted indicating a rotating stall cell. Such a distinction between stalled and unstalled blade flow regimes is not possible

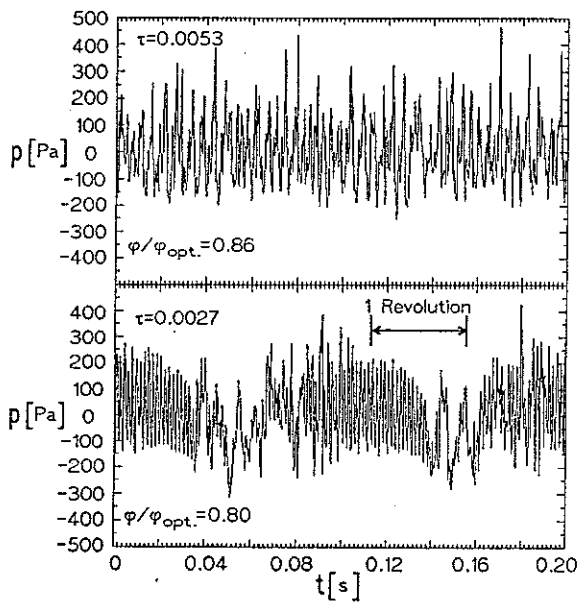

FIG. 11. Time history of wall pressure fluctuation under operating conditions with rotating stall for two tip clearance ratios, n=1400 rpm, ζ=-0.007.

for the trace obtained for larger tip clearance ratio (τ=0.0053) but note that in this case the general performance characteristic of the fan is also different from the smaller tip clearance in that it has no hysteresis region, compare Figure 2.

To ensure that the various spectral components discussed above are related to the rotation of the fan blades and not to acoustical effects, measurements were made at different impeller speeds, see Figure 12. Here the fluctuating pressures in the outlet duct (lower diagram) and at the casing wall (upper diagram) are normalized by $\frac{\rho}{2}U^2$, and the frequency by impeller diameter, tip speed and number of blades. With this definition of the Strouhal number, the blade passing frequency corresponds to St=1. The wall pressure was measured at the same location as before, and the operating condition is the one with the maximum tip clearance noise, i.e. φ=0.204 or $\varphi/\varphi_{opt.}$=0.93.

Figure 13 further illustrates the level variation of the blade passing frequency component and tip clearance noise with flow rate. Here the increase of the latter component from the point

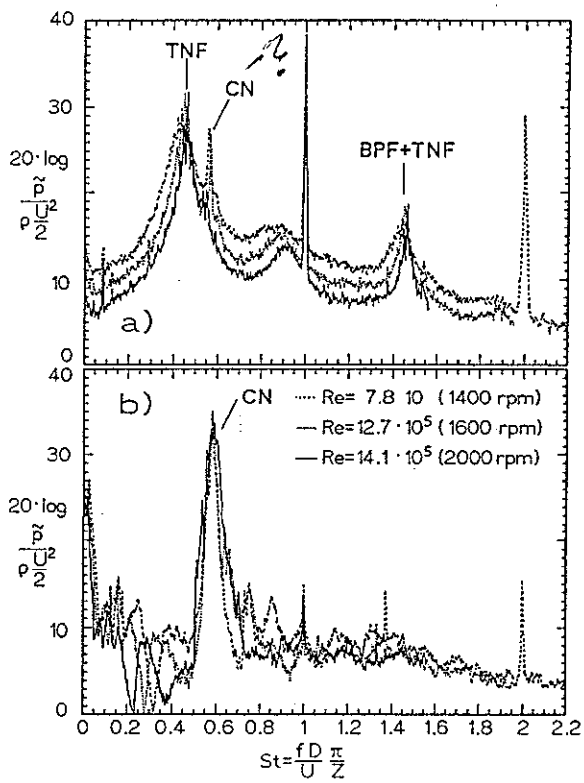

FIG. 12. Non-dimensional pressure spectra for various impeller speeds, a) outlet duct, b) casing wall (ζ=-0.007), $\varphi/\varphi_{opt.}$=0.93, τ=0.0053, Δf_b=1.56 Hz.

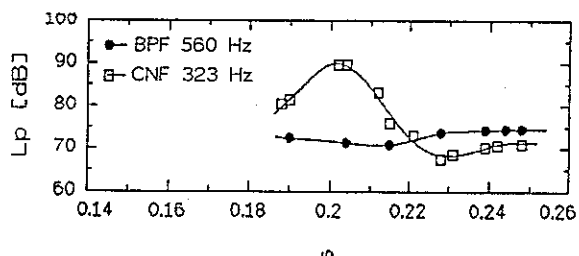

FIG. 13. Variation of blade passing frequency level (BPF) and tip clearance noise level (CNF) in the outlet duct as a function of the flow coeffizient, τ=0.0053, n=1400 rpm, Δf_b=1.56 Hz.

of maximum efficiency (φ=0.22) towards the last stable fan operating condition (φ=0.204, before the onset of rotating stall) is particularly evident.

In Figure 14 is shown how the level of various spectral components of the wall pressure fluctuation varies with axial distance from the rotor blade leading edges. The measured pressure level is corrected for the change in the free cross-sectional area at the various axial measurement positions. The operating point is again that of maximum clearance noise radiation into the acoustic far field. For all frequency components, the maximum level is found somewhat downstream the blade leading edge, i.e. at the location of maximum thickness of the impeller blades.

There is a similarity between the level variation of the tip clearance noise and the component at the difference frequency BPF-TNF which indicates once again that there is some correlation between these two spectral components, despite the fact that they are not of the same frequency. By comparison, all other components considered in Figure 14 decay much faster with distance from maximum blade thickness.

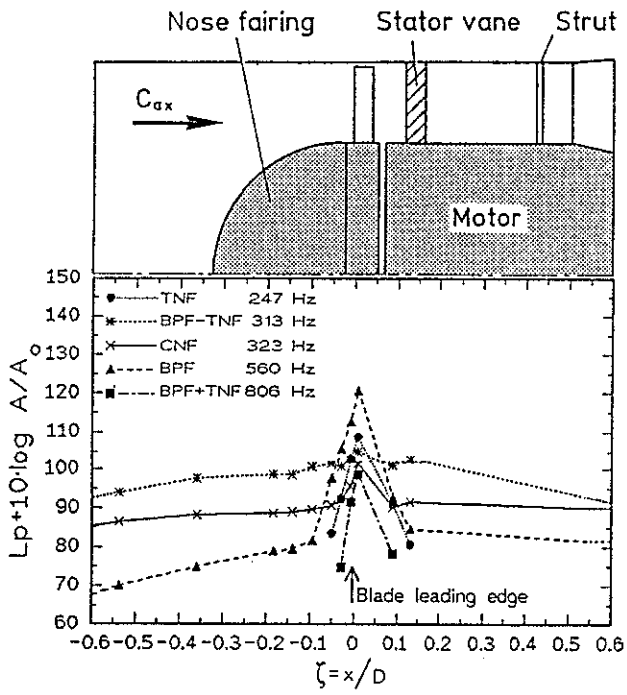

FIG. 14. Level of wall pressure fluctuations versus axial distance from the blade leading edges, τ=0.0053, $\varphi/\varphi_{opt.}$=0.93, n=1400 rpm.

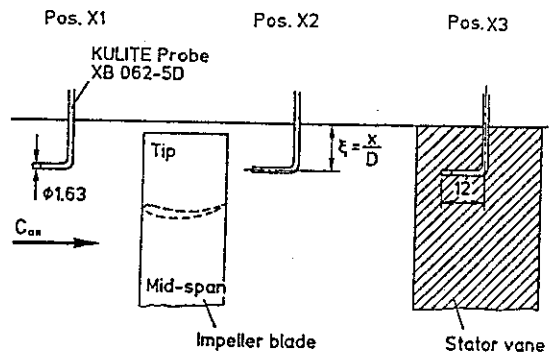

FIG. 15. Cross-section of the rotor-stator-region.

A simple-minded attempt was also made to measure fluctuating pressures in the presumed source region of tip clearance noise. For this purpose, an unsteady pressure probe (KULITE XB 062-5D) was inserted into the flow near the blade tip in a way similar to a Pitot-tube. The pressure sensing element is mounted at the stagnation point of the probe, compare the schematic shown in Figure 15. Figure 16 shows the spectra of the total pressure fluctuations in the flow for three different axial positions relative to the impeller; the radial distance from the wall was kept constant, ξ=x/D=0.022. Without discussing the exact nature and origin of the signal from this type of pressure probe, the level variation of the various spectral components is similar to that of the wall pressure shown in Figure 14: The turbulent noise component is significant only between rotor and stator and decays rapidly in the upstream and downstream axial direction. The level of the tip clearance noise component, however, is almost the same for the three axial measurement positions.

In Figure 17 the spectra of the total pressure fluctuations in the flow are described for three radial distances from the duct wall; the axial location is between rotor and stator (Pos. X2, compare Figure 15). The pressure level of the tip clearance noise does not change with distance from the wall, while the component termed turbulent noise exposes a maximum at ξ=0.029 which indicates that the source of this component lies near the blade tip.

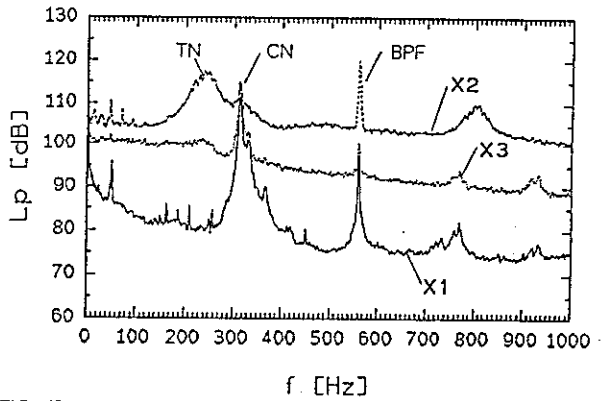

FIG. 16. Pressure spectra measured with KULITE-XB 062-5D probe at three axial positions ζ shown in Figure 15, X1 upstream of the impeller, X2 between impeller and stator vane, X3 in stator vane region, wall distance ξ=0.029, τ=0.0053, n=1400 rpm, Δf_b=1.56 Hz.

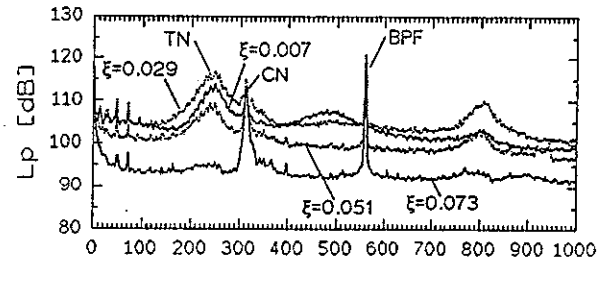

FIG. 17. Pressure spectra measured with KULITE-XB 062-5D probe at four radial wall distances, axial location X2, τ=0.0053, n=1400 rpm, Δf_b=1.56 Hz.

3.5 PRESSURE FLUCTUATIONS ON THE IMPELLER BLADES

To measure the fluctuating blade pressures, one impeller blade was equipped with four KULITE LQ 47-5 SG pressure sensors. Three of them are attached to the suction side and one to the pressure side, Figure 18 shows a schematic of the test arrangment. The pressure sensors are mounted in grooves milled into the blades, and a wax fairing ensured that the original blade geometry was retained. The sensor membranes are flush with the blade contour.

A comparison of the pressure spectra measured at the four blade positions is given in Figure 19 for a range of fan operating conditions and the largest tip clearance ratio τ=0.0053. The upper three diagrams (Figure 19 a-c) correspond to stable fan operating conditions, and the lower two to the rotating stall regime. In case of all four measurement positions, the spectra are dominated by spikes at the rotor frequency and multiples thereof which indicates that the stator vanes are not quite uniform in geometry or unevenly spaced. The stator vane frequency itself is not visible but buried in the random noise.

With rotating stall (Figures 19d-e), the low frequency random noise is increased, and harmonics of the stator frequency are masked. The spectra are now dominated by the rotating stall component with the highest levels at sensor location 2 and 3. This indicates that the blade flow is stalled first at the tip. When the flow is further reduced, the stalled flow regime extends deeper down to the hub. Note that the frequency of rotating stall component is now different from the one found in the wall pressure fluctuations (see Figure 9); the sum of the two frequencies is, of course, equal to the rotor shaft frequency. In Table 1 the frequencies measured in the fixed and the rotating frame of reference are compared.

φ	*fixed frame*	*rotating frame*
0.185	8.8 Hz	14.5 Hz
0.164	9.1 Hz	14.1 Hz
0.112	10.8 Hz	12.5 Hz

TABLE 1. Rotating stall frequencies in rotating and fixed frame of reference, τ=0.0053, n=1400 rpm.

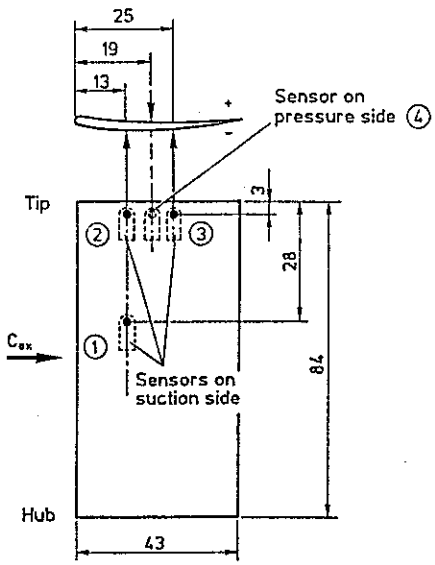

FIG. 18. Schematic of pressure sensors mounted on the impeller blade.

Closer to the hub (sensor 1), the pressure fluctuations are generally much lower in level than at the tip, except for the severely stalled fan operation condition depicted in Figure 19e. The spikes that dominate the signal from this sensor, on top of the rotor frequency harmonics, can be explained in part by

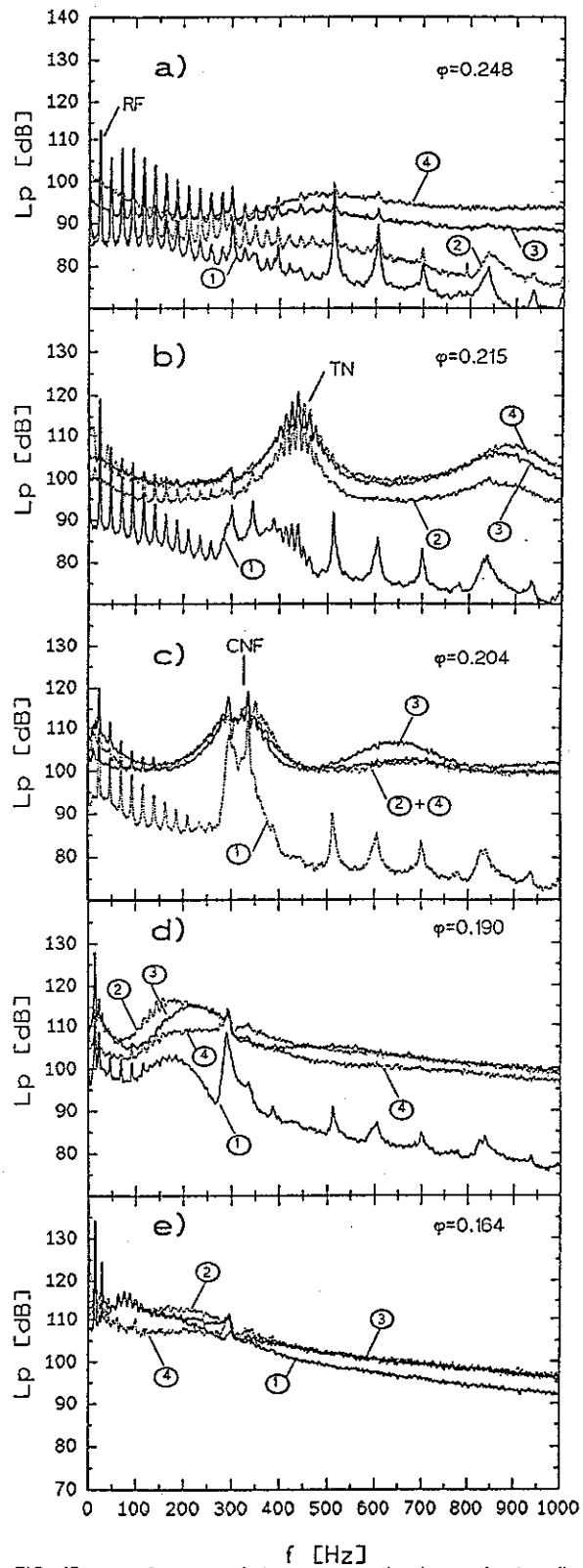

FIG. 19 a-e. Spectra of the pressure levels on the impeller blade for various operating conditions, τ=0.0053, n=1400 rpm, Δf_b=1.56 Hz.

acoustic resonance effects: The cut-on frequencies of the 1,0-mode and the 2,0 mode in the 280/450 mm diameter fan annulus are 296 and 591 Hz, respectively, and the 0,1-mode in the empty test duct (d=500 mm) is propagational at f≥830 Hz.

When the fan is operated just below the maximum efficiency point (φ=0.215), a broad band hump with superimposed multiple peaks appears in the spectrum which moves to lower frequencies when the flow is further throttled. This behavior is similar to that of the turbulence noise component in the wall pressure spectra, compare Figure 9. The frequencies measured in the fixed and in the rotating frame of reference, however, are different again.

The tip clearance noise component detected in the impeller blade pressure signal reaches its maximum level at a flow rate of φ=0.204, just as in case of the casing wall pressure fluctuations.

In Figure 20 is shown that the frequency variation of the various noise components goes in the same direction as the fan operating condition is varied, however, the rate of change is different. There is only one fan operating point for which the frequency difference BPF-TNF is equal to the frequency CNF of the tip clearance noise component.

In Figure 21 the turbulence noise component is analyzed with a higher frequency resolution to explore the discrete frequency peaks superimposed on the broad hump which have the character of a frequency modulation. In the upper diagram, non-dimensional spectra of the casing wall pressure are shown for three impeller speeds, and in the lower diagram the corresponding data for the impeller blade pressures are presented. One observation to be made is that the frequencies of the peaks vary linearly with the rotor speed and hence cannot be caused by acoustic resonance effects. This is true for both the wall pressures and the blade pressures. The frequency spacing of the peaks or, rather, the Strouhal number spacing ΔSt, are different in the rotating and the fixed frame of reference; the sum of the two, however, is equal to the dimensionless rotor shaft frequency: $\Delta St_{fixed} + \Delta St_{rot} = \frac{1}{Z} = \frac{1}{24}$.

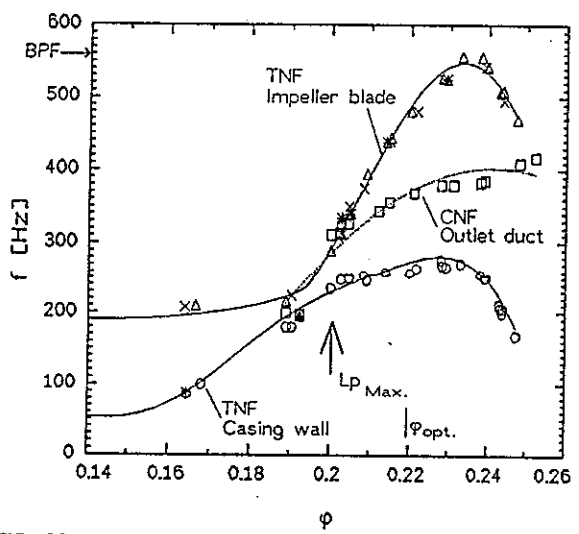

FIG. 20. Frequency variation of the pressure signals in the outlet duct (□, far field), at the casing wall (○, ζ=-0.007, near field), and on the impeller blade (① ≙ *, ② ≙ x, ③ ≙ Δ), τ=0.0053, n=1400 rpm, Δf_b=1.56 Hz.

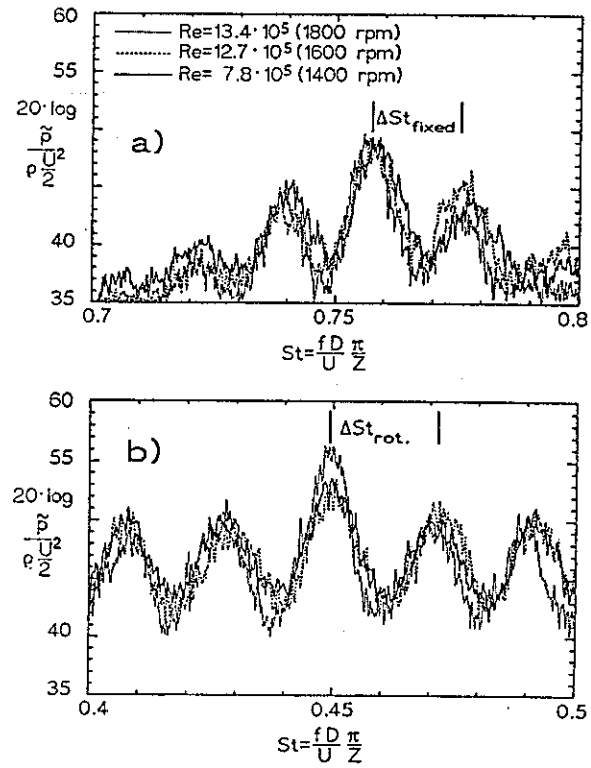

FIG. 21 a-b. Normalized pressure spectra for three Reynolds-numbers (rotor speeds), φ=0.215, Δf_b= 0.125 Hz,
a) measured at casing wall, ζ=-0.007,
b) measured on impeller blade position ④.

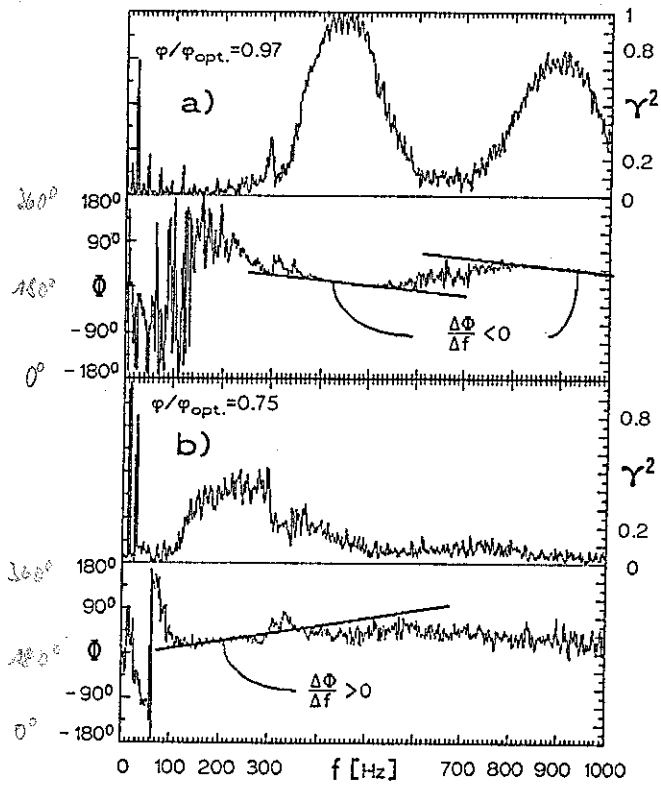

FIG. 22 a-b. Coherence γ^2 and phase angle Φ between the pressures measured on the pressure side ④ and the suction side ② of the impeller blade as a function of operating conditions, τ=0.0053, n=1400 rpm, Δf_b=1.56 Hz.

Figure 22 shows the coherence and the phase angle difference between the pressure measured on the suction side (3) and the pressure side (4) of one impeller blade, for two operating conditions. Close to the point of maximum efficiency (Figure 22 a) there is a strong correlation between the two signals in the frequency ranges around 450 Hz and 900 Hz. In these regions there is an almost linear change of phase angle Φ with frequency f. When the blade flow is stalled, the coherence of the two pressure signals is much lower, compare Figure 22b. Note that the gradient of the phase angle is now positive. In the case of the high coherence, the turbulence noise signal picked up by the pressure sensors is possibly generated by the secondary flow over the blade tip, i.e., the tip clearance flow. The lower coherence in Figure 22b can be explained by the blade flow separating from the suction side and moving across the blade channel to the pressure side of the next blade.

4. CONCLUSIONS

In this paper experimental results of an ongoing study are presented to identify the aeroacoustic generation mechanism of the noise related to the tip clearance flow in axial turbomachines which is driven by the pressure difference between suction side and pressure side of the blades. The measurements were made with an axial fan of 452 mm diameter and a hub tip ratio of 0.62. The number of impeller blades is Z=24, and the number of stator vanes V=17. The impeller size was kept constant in all experiments, and the tip clearance was varied by using casing segments of different diameter.

The aerodynamic and acoustic fan performance near the point of maximum efficiency is strongly influenced by the tip clearance. With a small clearance of τ=0.00067, the flow can be throttled to about 77 percent of the optimum flow rate before the fan's total pressure drops sharply. This drop is accompanied by a rise in the specific sound power level of up to 20 dB. Below this volume flow, the fan performance is characterized by a hysteresis in total fan pressure, sound power level, and efficiency. With a large tip clearance τ=0.0053, a drop in fan pressure and a hysteresis behavior are not found. A sudden change in noise level still exists, but not as large as before.

In the published literature higher broad band levels were reported when the tip clearance was enlarged. The present results show that in addition to that, significant sound pressure level increases occur within limited, almost narrow frequency bands in a region below the blade passing frequency component. The narrow-band level increases can be produced not only by increasing the gap while keeping the operating conditions constant, but also for one and the same tip clearance by throttling the flow over a certain limit. It is shown that these noise components are related to the interaction between flow separation on the blade suction side and the tip clearance flow.

When the volume flow is reduced further until the sudden changes in fan performance described above occur, the narrow-band peaks related to tip clearance noise in the far-field sound spectra dissappear, while low frequency components rise substantially; this is the reason for the drastic increase in total sound power.

Measurements of wall pressure fluctuations adjacent to the blade tip localize the generation of tip clearance noise in the impeller region. Pressure measurements on one impeller blade have shown the existence of frequency components caused by turbulent flow in the tip region of the blade. These turbulent pressure fluctuations show the same characteristic behavior in the fixed system and in the rotating system, but their frequencies are different and are related to one another in a way not yet unterstood.

Additionally, the rotating stall frequencies measured in the fixed and in the rotating system are modulations of the rotor frequency. In fact the sum of both equals the rotor frequency, independent of operating conditions or rotor speed.

In the next phase of the study, flow visualisation and hot-wire measurements of the gap flow will be made. It is hoped that more detailed information about the flow velocity components in the tip region of the impeller will provide further insight into the generation mechanism of the tip clearance noise.

5. REFERENCES

[1] LONGHOUSE, R.E.: Control of tip-vortex noise of axial flow fans by rotating shrouds, Journal of Sound and Vibration 58 (2), 201-214, 1978.

[2] MARCINOWSKI, H.: Einfluß des Laufradspaltes und der Luftführung bei einem Kühlgebläse axialer Bauart, MTZ 14, 259-262, 9/1953.

[3] STÜTZ, W.: Experimentelle Untersuchung zum Radialspalteinfluß auf das aerodynamische und akustische Verhalten eines Axialventilators. Strömungsmechanik und Strömungsmaschinen 39, 153-160, Karlsruhe 1989.

[4] FUKANO, T.; TAKAMATSU, Y.; KODAMA, Y.: The effect of the tip clearance on the noise of low pressure axial and mixed flow fans, Journal of Sound and Vibration, 105(2),291-308,1986.

[5] KAMEIER, F.; GEUER, U.; NEISE, W.: Untersuchung zur Entstehung des Blattspitzen-Wirbellärms an einer axialen Strömungsmaschine, VDI Berichte Nr. 872, 343-358, 1991.

[6] ISO/DIS 5136.2: International Organisation for Standardization, Draft International Standard, Acoustics - Determination of sound power radiaded into duct by fans - In-duct method, 1985.

[7] DIN 45 635, Teil 9: Geräuschmessungen an Maschinen, Luftschallmessung, Kanal-Verfahren, Rahmen-Meßverfahren für Genauigkeitsklasse 2, 12/1989.

[8] INOUE, M.; KUROUMARU, M.; IWAMOTO, T.; ANDO, Y.: Detection of a rotating stall precursor in isolated axial flow compressor rotors, Journal of Turbomachinery, Vol. 113, 281-289, 1991.